

A Virtual-Reality Driven Approach for Generating Humanoid Multi-Contact Trajectories

Stephen McCrory^{1,2}, Sylvain Bertrand^{1*}, Duncan Calvert^{1,2}, Jerry Pratt³, Robert Griffin^{1,2}

Abstract—We present a virtual reality (VR) framework designed to intuitively generate humanoid multi-contact maneuvers for use in unstructured environments. Our framework allows the operator to directly manipulate the inverse kinematics objectives which parameterize a trajectory. Kinematic objectives consisting of spatial poses, center-of-mass position and joint positions are used in an optimization based inverse kinematics solver to compute whole-body configurations while enforcing static contact stability. Virtual “anchors” allow the operator to freely drag and constrain the robot as well as modify objective weights and constraint sets. The interface’s design novelty is a generalized use of anchors which enables arbitrary posture and contact modes. The operator is aided by visual cues of actuation feasibility and tools for rapid anchor placement. We demonstrate our approach in simulation and hardware on a NASA Valkyrie humanoid, focusing on multi-contact trajectories which are challenging to generate autonomously or through alternative teleoperation approaches.

I. INTRODUCTION

Humanoid robots are frequently designed to be capable of a wide range of motions. Making full use of these platforms as well as understanding their limitations requires an ability to generate and deploy coordinated, multi-contact maneuvers. Generating such motions requires relaxing assumptions about the robot’s posture and contactable limbs in order to maintain generality. The application of search-based planning to this problem presents a number of obstacles. Primarily, multi-contact motions have an inherently large branching factor which can cause planning to be computationally intractable or rely on heuristics [1, 2]. Additionally it is challenging to construct generalized posture scoring functions that perform well over a large space of configurations. Alternatively, operator-driven approaches have been proven as a reliable means of commanding complex humanoid motion [3–5]. With many recent successful results using virtual reality (VR) [6–10] we believe it is a well-suited solution to the problem of generating multi-contact humanoid trajectories.

In this paper we present a VR-based framework which enables the operator to create whole-body trajectories by iteratively posing the robot in contact stable, collision-free configurations. This is achieved by mapping kinematic objectives to virtual elements which can be easily created, removed or modified by the operator. The aim of this design

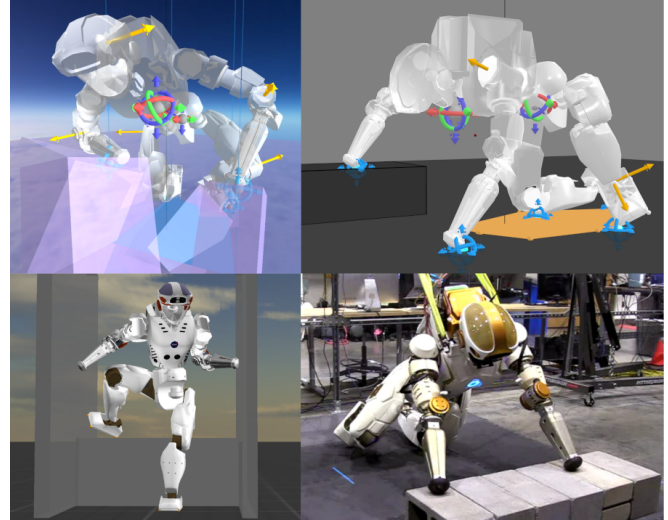


Fig. 1: Demonstration of the presented motion generation framework on Valkyrie in various multi-contact scenarios. The virtual reality application (top-left) enables the operator to iteratively create key frames by dragging the robot to the desired configuration. The desktop application (top-right) is used for editing and analysis of trajectories. Trajectories are validated in simulation (bottom-left) and hardware (bottom-right) on the Valkyrie humanoid.

is creating a system with sufficient generality for use in a wide range of motions and contact modes. Following this approach, the operator can constrain any rigid body or joint and the framework makes no assumptions about the robot’s posture or contacting limbs. This represents a design trade-off by creating higher operator burden in exchange for increased operator expressiveness. We make this design choice in order to have a single framework for handling many multi-contact scenarios, such as crawling, climbing, leaning, rolling and kneeling. To test our framework, we generate trajectories for a set of diverse multi-contact scenarios and validate them in simulation and hardware on a NASA Valkyrie humanoid.

The main contributions of this framework are in the implementation of the VR UI and the generality of motion generation (Section V):

- 1) A generalized use of interactable constraint anchors which contain no assumptions of the environment or preferred posture.
- 2) Automated constraints and visual cues for CoM feasibility through an actuation-aware constraint region and force polytopes.
- 3) An intuitive mechanism for generating robot-environment contact constraints.

¹Author is with the Institute of Human and Machine Cognition (IHMC), 40 S Alcaniz St, Pensacola, FL 32502, USA author@ihmc.org

²Author is with the University of West Florida (UWF), 11000 University Pkwy, Pensacola, FL 32514, USA author@uwf.edu

³ Author is with Figure AI, Inc., Sunnyvale, CA

* The author initiated this project.

This work was supported through ONR Grant No. N00014-19-1-2023 and NASA Grant No. 80NSSC20M0197.

II. RELATED WORK

Translating an operator’s intent to robot motion is a challenging task, particularly when commanding coordinated motions to legged or dexterous robots. This challenge has given rise to various retargeting frameworks for efficiently mapping operator input to robot motion. Methods for retargeting depend on factors such as available human measurements, task application and control scheme [6].

One approach is to use a simple map to give the operator direct control of the mapped task. In Leeper et al. [11] this is implemented through an interactable “rings-and-arrows” widget that directly maps to the controller’s end-effector setpoint. Similar strategies of direct setpoint control were widely used during the DARPA Robotics Challenge for teleoperating humanoids [3–5]. In these frameworks, the operator directly interfaced with an inverse kinematics solver’s setpoint through similar interactable elements. These approaches, in particular [5], also had additional flexibility such as selecting hand, chest, pelvis and Center of Mass setpoints as well as the taskspace constraint set and base of the kinematic chain. Recently this approach has been adapted to VR for use in humanoid teleoperation [7, 8]. In Wonsick et al. [8] the operator places hand waypoints in the world which can be freely adjusted before planning an arm trajectory.

The use of VR and motion capture enables more sophisticated operator mapping such as partial- or whole-body kinematic retargeting. Early pioneering work by Pollard et al. [12] used motion capture data from a human actor to mimic dancing motions by mapping to the torso and upper body of a fixed-base humanoid. The operator-to-robot mapping accounted for joint limits, velocity limits and singularities. Extensions of this work include online reference motion for enabling upper-body dancing with active balance [13] and simulated stepping and Tai-chi maneuvers [14]. Recently, there have been integrated architectures in which the operator commands reference postures through a retargeting scheme and walking behavior through a joystick or treadmill [9, 10, 15]. These architectures have had success in tasks requiring both walking and manipulation such as door opening, wall bracing and debris removal. In Otani et al. [16] a motion capture based retargeting scheme is applied to multi-contact manipulation scenarios. Operator motion is mapped to support, free and manipulation tracking sets and is demonstrated in simulation by bracing against a table while manipulating an object.

III. ARCHITECTURE

The diagram in Fig. 2 shows the control flow of our framework. At a high level, the operator creates whole-body trajectories by incrementally generating statically stable, collision-free key frames. These key frames can either be created offline using a simulation or online with hardware and are logged for future editing and reuse. At a software level, there are three processes involved in generating trajectories. The first is the user-interface (UI) which enables the operator to specify kinematic objectives and validate key frames. Both a VR app in Java Monkey Engine [17] and a desktop app in

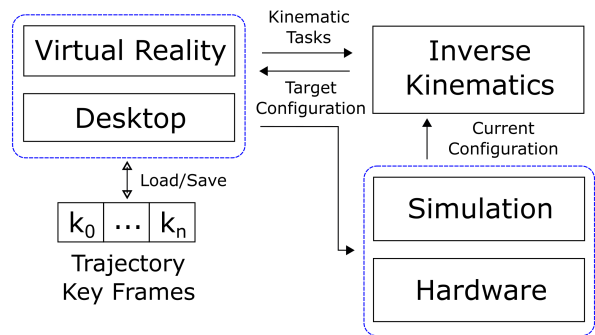


Fig. 2: High-level architecture of the motion generation framework. Solid arrows designate ROS 2 messages which are sent between modules. Hollow arrows designate saving and loading to file. Blue dashed lines represent a message-level layer of abstraction.

JavaFX [18] are implemented with similar functionality. In practice, the VR UI is preferred for generating trajectories from scratch and the desktop for editing existing trajectories. The VR app is developed for the Valve Index [19] and also has bindings for the HTC Vive [20]. The second process is an optimization-based inverse kinematics solver (Sec. IV) which solves for whole-body configurations given a set of kinematic objectives. The third process is a robot controller which executes the commanded motion in either a physics simulator or on hardware. Both the UI and robot controller have message-layer abstraction to allow any permutation of active modules (Fig. 2). All inter-process communication is done through ROS 2 messages [21].

IV. INVERSE KINEMATICS SOLVER

An optimization based inverse kinematics solver is used to compute whole-body configurations based on the operator’s input. We solve the IK problem using sequential quadratic programming (SQP) due to its generality and success on humanoids [22, 23]. The IK iteratively solves the following quadratic program (QP):

$$\begin{aligned} \min_{\mathbf{v}_d} \quad & c_{\text{nom}} + \mathbf{c}_J + c_{\mathbf{v}_d} \\ \text{s.t.} \quad & \mathbf{v}_{\min} \leq \mathbf{v}_d \leq \mathbf{v}_{\max} \\ & \mathbf{A}\mathbf{v}_d \leq \mathbf{H} \end{aligned} \quad (1)$$

The objective function terms are given by:

$$\text{Nominal Objective: } c_{\text{nom}} = (\mathbf{v}_d - \mathbf{v}_{\text{nom}})^T \mathbf{C}_{\text{nom}} (\mathbf{v}_d - \mathbf{v}_{\text{nom}})$$

$$\text{Kinematic Objective: } c_J = (\mathbf{J}\mathbf{v}_d - \mathbf{p})^T \mathbf{C}_J (\mathbf{J}\mathbf{v}_d - \mathbf{p})$$

$$\text{Velocity Cost: } c_{\mathbf{v}_d} = \mathbf{v}_d^T \mathbf{C}_{\mathbf{v}_d} \mathbf{v}_d$$

Where the terms are given by:

- \mathbf{v}_d is the vector of desired joint velocities
- \mathbf{v}_{nom} drives the robot to a nominal whole-body configuration.
- $\mathbf{J} = [\mathbf{J}_1^T \dots \mathbf{J}_k^T]^T$ and $\mathbf{p} = [\mathbf{p}_1^T \dots \mathbf{p}_k^T]^T$ are the stacked Jacobian matrices and motion objectives computed as feedback terms from desired kinematic objectives, which is detailed below.

- \mathbf{v}_{min} and \mathbf{v}_{max} bound the joint velocity. A nominal set of bounds are used unless a joint is near a limit, in which case the velocity is constrained such that the joint remains within its range of motion within the update tick ΔT .
- \mathbf{A} is the linear centroidal momentum matrix [24] and $\mathbf{h} = \mathbf{A}\mathbf{v}_d$ is the linear momentum. \mathbf{H} constrains the centroidal momentum to such that the CoM remains inside the support region.
- \mathbf{C}_{nom} , \mathbf{C}_J , and \mathbf{C}_{v_d} are positive diagonal weight matrices.

The term *controller robot* denotes the real or simulated robot running a controller and the term *puppet robot* denotes the model which the inverse kinematics solver updates (due to its role in the interface, see Sec. V). The puppet model initializes to the controller robot’s current configuration and the QP in Eq. (1) is iteratively solved until the cost term converges or a maximum number of iterations is reached. With each iteration, the puppet model is updated by integrating the computed velocities according to Eq. (2).

$$\mathbf{q} \leftarrow \mathbf{q} + \mathbf{v}_d \Delta T \quad (2)$$

A. Motion Tasks

A set of motion tasks are computed from the desired kinematic tasks. The motion task with index i is given by:

$$\mathbf{J}_i \mathbf{v}_d = \mathbf{p}_i \quad (3)$$

A motion objective \mathbf{p}_i is computed from a feedback controller on a desired kinematic task. Kinematic tasks consist of:

- Joint position, in which \mathbf{J}_i is a selection matrix for the joint and \mathbf{p}_i is a velocity towards a desired position.
- Center of Mass (CoM) of the robot, in which a desired CoM position in world is specified. The Jacobian is the linear centroidal momentum matrix \mathbf{A} and the objective \mathbf{p}_i drives towards the desired CoM position.
- Spatial pose of a rigid body, in which a desired position and orientation in world and corresponding frame fixed to the rigid body are specified. A proportional feedback law on the error transform is used to compute \mathbf{p}_i [25].
- Environment collision avoidance, in which \mathbf{J}_i is the jacobian of a detected collision point and \mathbf{p}_i is a velocity separating the collision.

For the CoM and spatial pose tasks, a selection matrix \mathbf{S}_i can be used to constrain certain spatial components of a task. This is done by premultiplying both the Jacobian and objective by \mathbf{S}_i . Motion tasks have a corresponding weight matrix \mathbf{w}_i , such that \mathbf{C}_{nom} , \mathbf{C}_J and \mathbf{C}_{v_d} have the block-diagonal form:

$$\mathbf{C} = \text{diag}(\mathbf{w}_0, \dots, \mathbf{w}_k) \quad (4)$$

This formulation is adopted from [26], which details the calculation of motion objectives and feedback controllers.

B. Environment and Collision Modelling

Robot and environment collision meshes are modelled as a set of convex polytopes and the environment polytopes are assumed to be known. Robot polytopes are attached to a corresponding rigid body and environment polytopes are fixed in world. The Expanding Polytope Algorithm (EPA) is used to check for collisions between pairs of polytopes [27]. This algorithm provides additional data such as nearest points in the absence of a collision and maximum penetrating points in the presence of a collision. During each iteration of the IK all pairs of robot and environment meshes are checked for collisions. Any detected collision is converted to a high-weight feedback command which separates the colliding meshes.

C. CoM Constraint Region and Contact Force Polytopes

The CoM constraint region used to compute \mathbf{H} can be constructed by either a simple flat ground contact model or by including the environment mesh in the contact model. For the flat ground model, the CoM is constrained to the convex hull of the robot’s contact points. For scenarios where the robot is not in flat ground contact, the IK can compute a generalized support region. This constraint region follows the approach by Bretl et al. [28] to compute a friction-consistent region and its extension in [29] to include actuation constraints. The region is approximated by solving a series of Linear Programs in which friction and actuation limits are included as inequality constraints. To model the actuation constraints for a contact point i , a force polytope \mathcal{P}_i is computed which represents the set of actuation-consistent forces at the contact point [30]:

$$\mathcal{P}_i = \{\mathbf{f}_i \in \mathbb{R}^3 \mid \underline{\tau} \leq \mathbf{J}^T \mathbf{f}_i \leq \bar{\tau}\} \quad (5)$$

Where $\underline{\tau}$ and $\bar{\tau}$ are the lower and upper torque bounds along the contacting limb and \mathbf{J} is the Jacobian of the contact point. We compute the vertices of the force polytope by projecting each actuation limit τ_{lim} using the pseudoinverse of the contact Jacobian to get the corresponding force \mathbf{f}_{lim} .

$$\mathbf{f}_{lim} = (\mathbf{J}^T)^\dagger \tau_{lim} \quad (6)$$

For a limb with n joints, the force polytope is backed out by iterating through each permutation of the 2^n values of τ_{lim} . In addition to being used to compute the CoM constraint region, the contact force polytopes are provided as visual cues to the operator.

V. VIRTUAL REALITY USER INTERFACE

The VR user-interface is designed to enable an operator to pose the robot by creating and modifying constraints on-the-fly. To do this, we implemented virtual interactable “anchors” which correspond to kinematic tasks. Fig. 3a shows the robot in a squatting configuration which has anchors on the chest, legs and arms. The interface displays two robots: a transparent puppet robot which the operator manipulates and (optionally) an opaque controller robot.

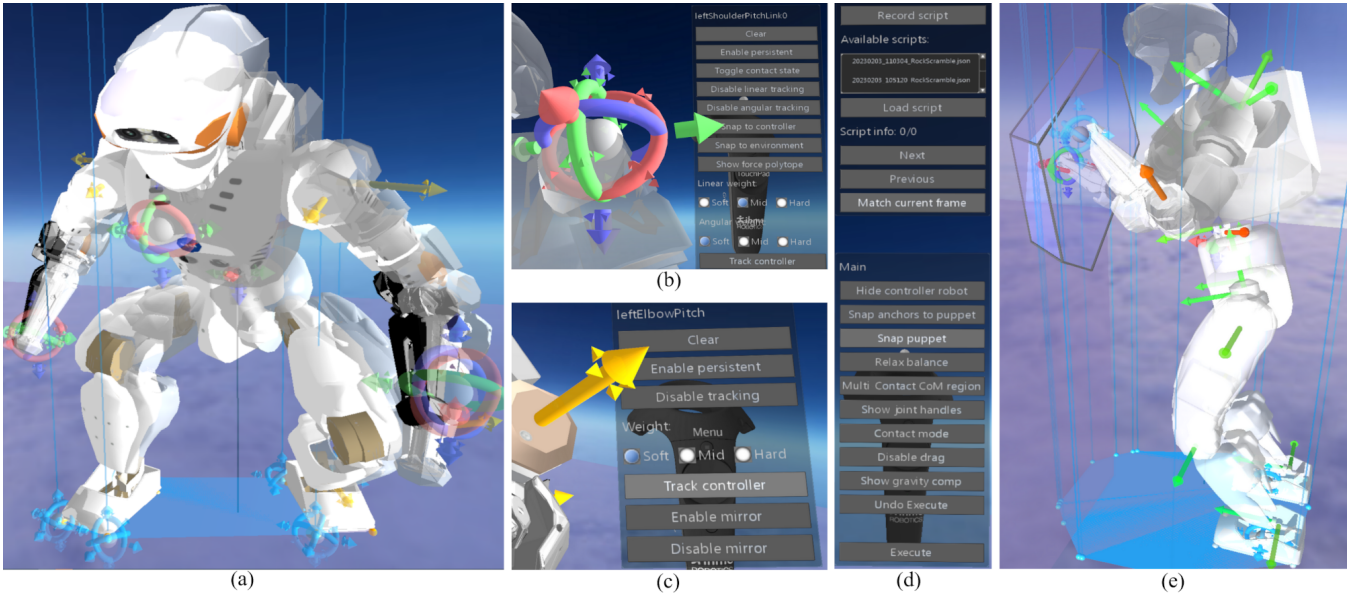


Fig. 3: (a) Operator view while using the VR interface to pose Valkyrie in a squatting position. The robots and anchors are fixed in the scene and the operator can walk or teleport to move around. (b) A spatial pose anchor and its corresponding menu panel. (c) A joint position anchor and its corresponding menu panel. (d) The main menu is used to export or load scripts, toggle visibility of the controller robot and joint position anchors, configure the IK solver behavior, and change anchor behavior by toggling contact mode and dragging. (e) Valkyrie braced against a wall with the left arm and reaching with the right arm. Visual cues for actuation feasibility include force polytopes, actuation and friction consistent support region, and alerts for joints at risk of torque saturation.

A. Anchor Configuration

The interface contains three types of motion control anchors: spatial pose, Center of Mass, and joint position. Spatial pose anchors are created by simply clicking on the desired rigid body and dragging it to the desired pose. Individual axes can also be activated, cleared or modified. A “ring-and-arrows” [11] indicates the anchor setpoint, with actively constrained axes highlighted (Fig. 3b). Spatial pose anchors can be designated as a “contact anchor”, shown as smaller, blue anchors, which increases the weight and can be used to construct the support region (see V-B). The CoM anchor is represented by only arrows since there is not an orientation setpoint but is modified in the same way as the spatial pose. Joint position anchors are a single arrow centered at the joint. When dragging the joint, vertical motion in world frame is mapped to a desired joint position.

Each anchor has a menu with additional customization options. Figures 3(b) and 3(c) show the spatial pose and joint position menus, respectively. Each menu allows switching between low, medium and high weight for the corresponding kinematic task, which corresponds to entries of C_J in the IK. Each anchor can optionally be set to match the controller robot’s pose. Two options are provided: a tracking option which continuously updates to the controller’s pose and a snapping option which performs the update once. The tracking feature is beneficial for any contact that does not need precise placement in world frame but needs to remain stationary. Each anchor can also be flagged as “persistent,” such that the user can quickly clear all anchors which are not persistent. We find that often the operator would keep certain anchors static while iterating through configurations

of other anchors and a notion of persistence aids the operator in this process. The joint position anchor has a “mirroring” option in which dragging or activating a joint will perform the same action on the opposite-side joint, if one exists.

Spatial pose contact anchors are created in a specific way to ensure the robot and environment mesh polytopes are in contact and tangent, shown in Fig. 4. The operator first enables “contact mode”, in which the controller is then projected to the surface of the nearest robot mesh as the operator moves (Fig. 4(a)). The surface normal of the robot mesh is also shown during this step. When the operator chooses a contact point, the controller then switches to projecting to the environment mesh, with that surface normal also being shown. When the operator chooses a setpoint, the contact point then snaps to this position. We note that the orientation is only constrained in the two orientations required to keep the polytopes tangent. This is achieved by first having the z axis of the task frame aligned with the robot mesh surface normal. The x and y orientation setpoints are then computed to align the two surface normals.

B. Actuation Feasibility

The interface is intended for multi-contact scenarios which may saturate the robot’s actuation limits. Visual cues are included to assist the operator in maintaining actuation feasibility, shown in Fig. 3(e). The force polytope [30] of any contact point can be visualized and is updated as the robot’s posture is adjusted. This can be useful when the “major axis” of the polytope has an intuitive orientation, such as vertical when contacting the ground or horizontal when bracing against a wall. A multi-contact support polygon can

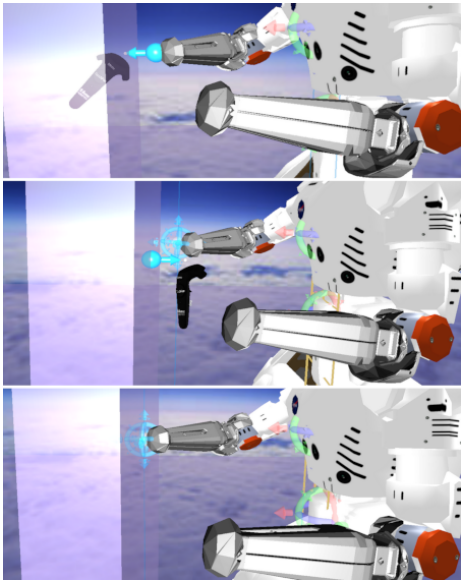


Fig. 4: Contact points are projected to the surface of the collision mesh while creating and placing a contact anchor. The arrow indicates the surface normal of the robot or environment mesh.

also be visualized for cases where the feasibility of the CoM position needs to be checked. This region is a convex set of feasible CoM XY positions based on the contact friction constraints [28] and actuation constraints [29] of the robot. The operator can toggle between this generalized support region and the nominal convex hull of contact points. The active support polygon is also sent to the inverse kinematics module to compute \mathbf{H} , to constrain the robot’s CoM. A visualization of the feasibility of individual joint torques for the target configuration is also provided. Given the robot’s contact state, we compute the torques required for static equilibrium through inverse dynamics. The color of each joint anchor from this to provide a visual cue for joints which are near saturation. For example, the elbow joint in Fig. 3(e) is red, indicating it is near a torque limit for this configuration.

C. Additional Operator Tools

An option to “snap anchors to puppet” is provided which replaces each anchor’s setpoint with the achieved value of the IK solver. For tasks with numerous anchors this is a tool for ensuring the operator is requesting a feasible set of objectives. The operator can also “snap puppet” when a preferred configuration is reached, which sets the kinematic solver’s nominal configuration (Sec. IV) to the current solver solution. This was found to be helpful during manipulation tasks where the arm’s nullspace may not be sufficiently constrained.

D. Interface Workflow

The trajectory design workflow has three phases: prototype, edit and deploy. We primarily prototype in simulation but the framework does allow for online trajectory creation (Fig. 2). When prototyping, the puppet robot is initialized

to the controller robot’s configuration and operator begins placing anchors. When the desired pose is reached, the operator dispatches the pose to the controller which executes the motion. The key frame is also stored which includes the controller robot’s pose, the puppet robot’s pose and all anchor data. If the operator is not satisfied with the motion or the robot falls down, an “undo” button is available which rewinds the simulator to the start of the motion and removes the stored key frame. This process is iteratively performed until the trajectory is complete, which usually is comprised of 5-20 key frames. The list of key frames as well as environment model is logged as a JSON file. Trajectory scripts can be edited and replayed in both the VR or desktop applications. Often it is useful to prototype a “template” script from which other scripts can be created. For example, a push-up template can be copied and push-ups of varied heights can be achieved by only modifying the \mathbf{z} setpoint of the CoM objective. In the following section we present results from deploying trajectories in simulation and on hardware.

VI. POST-PROCESSING AND CONTROL

In order to execute a given motion, the key frames are converted to a continuous jointspace trajectory $\mathbf{q}(t)$ which can be tracked by a controller. This trajectory is constrained by the list of key frame configurations $\mathbf{q}_0 \dots \mathbf{q}_n$ and key frame times $t_0 \dots t_n$, such that $\mathbf{q}(t_i) = \mathbf{q}_i$. We model the trajectory as a sequence of third-order polynomial splines between key frames and enforce position and velocity continuity between splines. This results in $n - 2$ free variables for the velocity at each key frame, given the start and end velocities are constrained to the controller robot’s current velocity and zero, respectively. The following optimization is solved to compute the unconstrained key frame velocities $\dot{\mathbf{q}}_u$, where $q_i(t)$ is the scalar trajectory of joint i :

$$\min_{\dot{\mathbf{q}}_u} \sum_i \int \|\dot{q}_i(t)\|^2 dt \quad (7)$$

The trajectory $\mathbf{q}(t)$ is tracked using an impedance controller consisting of a PD tracking law with an optional gravity compensation term. For trajectories where the contact state is trusted the gravity compensation is enabled. However for highly contact-rich motion such as scenarios (c) and (e) in Table I, gravity compensation is disabled.

VII. RESULTS

We tested our framework by generating motions for a variety of multi-contact scenarios. Table I contains some of these scenarios along with key frame statistics. All trajectories were validated in simulation and trajectories (e) and (f) were validated on hardware. Key frame transitions have a default value of 2s for simulation and 4s for hardware but the operator can override this value to both shorten or extend transitions. We selected contact-rich scenarios to generate motions that are difficult to plan autonomously or through standard teleoperation. Many of the robot’s limbs are used for contact, including feet (all), arms (all), knees (a, c, d, f), and chest (c, d). Additionally, many contact

TABLE I: Trajectories validated on the Valkyrie humanoid in simulation (all) and hardware (e, f).

	Description	Number of key frames	Duration (s)	Number of unique non-contact 6-dof anchors	Number of unique contact 6-dof anchors	Number of unique 1-dof anchors	Number of unique CoM anchors
(a)	Standing up from lying down on flat ground	22	57.5	22	18	53	16
(b)	Stepping over a 45cm tall barrier with handholds	18	59	14	38	38	17
(c)	Climbing up and standing on an 80cm tall ledge	24	61.5	16	27	32	20
(d)	Rolling over from facing down to facing up	6	19.5	3	7	45	0
(e)	Reaching forward and bracing against a wall to extend range of motion	5	25	6	9	1	3
(f)	Crawling to kneeling with flat handholds	21	84	24	27	47	18

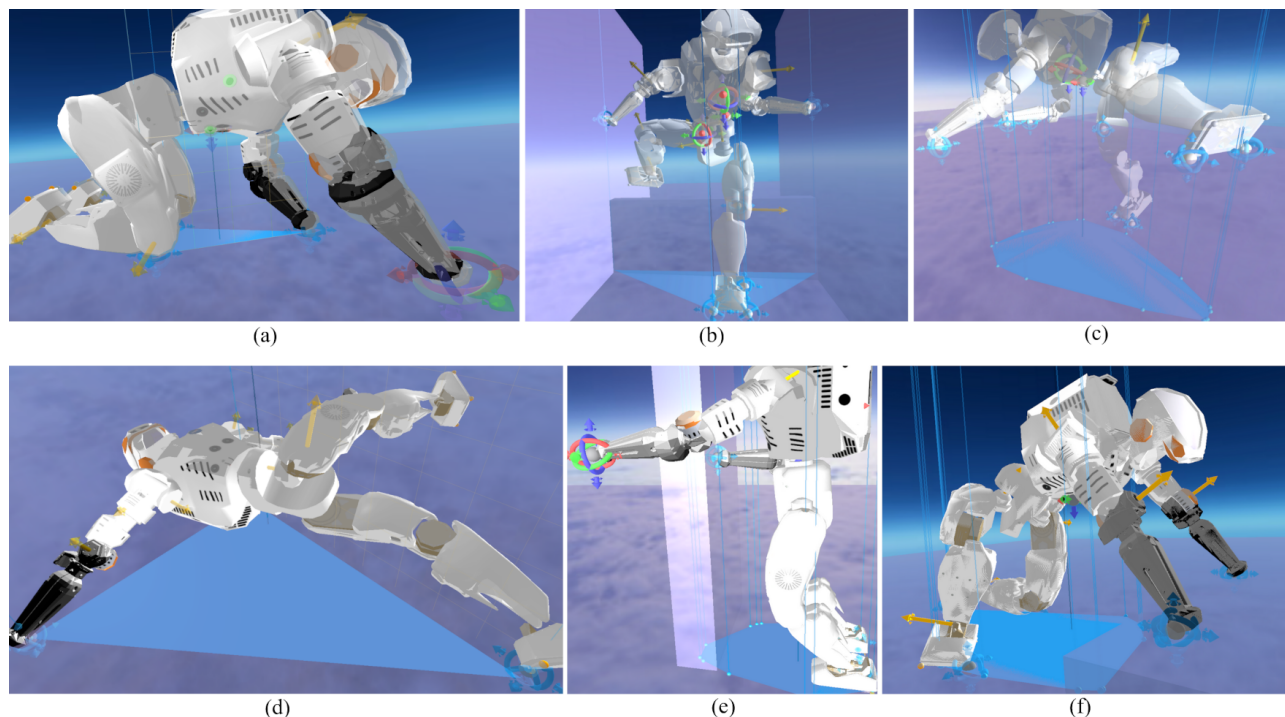


Fig. 5: Operator view while generating trajectories.

geometries are included. Planar contact occurs when the foot is in full contact with the environment. Point contacts are also common when the arms or knees are in contact with the environment, since these are modelled using curves meshes. Line contacts are also used when one edge of the foot is in contact, such as both feet in Fig. 5(c). We find that the operator’s use of anchors varies significantly based on the scenario. For example, when rolling over on flat ground (scenario d) the robot is often in a position where the CoM cannot be directly controlled and was not used as an anchor. In contrast, climbing onto a ledge (scenario c) requires careful positioning of the CoM while climbing and therefore is used in almost every key frame.

A. CoM Constraint Regions

To validate effectiveness of the CoM constraint region (Sec. V-B) for the generated motions, we compare it to a baseline flat-ground constraint. Figure 6 shows this comparison performed for scenarios (e) and (f). The “flat ground” model computes the constraint region as the convex hull of the robot’s contact points. The “multi-contact” constraint region is computed using the friction- and actuation-aware model. The plotted quantity is the distance of the CoM to the nearest constraint edge of both regions. Both scenarios have key frames with substantial (multiple centimeter) difference in stability margin. Although the multi-contact constraint region is generally more restrictive, scenario (e) key frame 2 demonstrates this is not always the case. This key frame corresponds to a braced reaching motion, shown in Figure

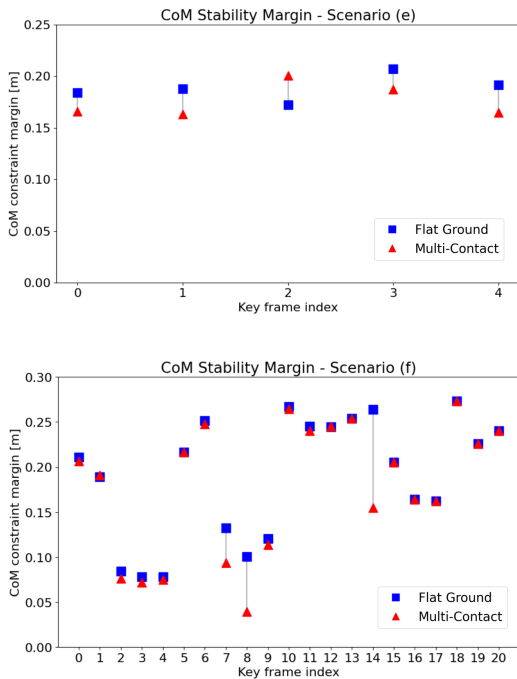


Fig. 6: CoM stability margins for scenarios (e) and (f).

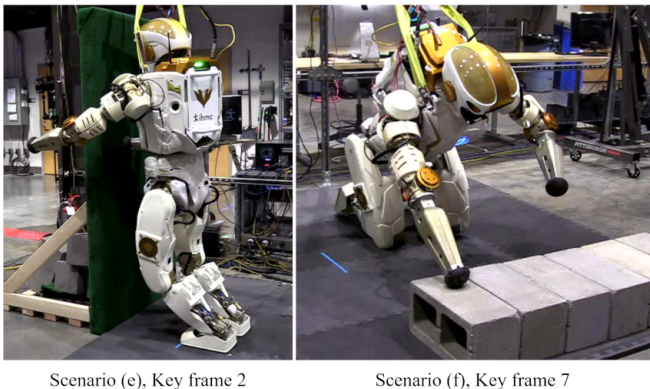


Fig. 7: Valkyrie executing two multi-contact motions: (left) bracing against a wall with the right arm and reaching forward with the left arm and (right) placing the arms on cinder blocks while maneuvering to a kneel.

7 (left). In this situation, using the multi-contact constraint region enables a higher range of motion than would be possible if using the flat-ground model. Conversely, the multi-contact region is very restrictive for configurations in scenario (f) that require support from the arms. In scenario (f) key frame 7 (Fig. 7), the robot places significant weight on the right arm while lifting the left arm. The actuation limits of the right arm are reflected by the multi-contact constraint being 5cm higher than the flat ground model.

B. User Interface Operation

We find there are two primary reasons for a generated key frame to be infeasible: controller failures and inverse kinematics failures. Controller failures often occur because the CoM trajectory is unstable or there is an unexpected

collision while moving to a key frame. Our approach assumes that key frames are sufficiently close such that validating subsequent key frames serves as a validation of the trajectory between them. However in practice this does not always hold, particularly when a limb is moving near the environment such as the foot moving over the barrier in Fig. 5(b). This could be addressed by incorporating a motion preview similar such as [4, 5]. Inverse kinematics failures occur for two reasons: getting “stuck” and going unstable. Since our IK solver is based on local optimization, it is susceptible to getting stuck in local minima. Often the operator can guide the robot out of the minimum when aware that the problem is occurring. Solver instability can occur when inconsistent objectives are requested with high weight, such as contacts, collisions and CoM positioning. Such cases require halting the IK and reverting to the last key frame. For this reason, the operator may prefer disabling CoM and collision constraints in the solver and using visual cues as indication of feasibility, which can mitigate solver instability.

VIII. DISCUSSION AND FUTURE WORK

Using the presented VR-based framework, we were able to generate a wide variety of feasible multi-contact humanoid trajectories. The ability to generate complex trajectories from scratch has applications to many areas of robotics, such as informing both mechanical design and controller design through simulations and deployment during teleoperation. Our main design choice was a user interface that makes minimal assumptions of the motion and relies on an operator for all kinematic objectives. We believe this high level of operator burden can be mitigated in future work which could in turn reduce motion generation time. One approach could be to predict the subsequent key frame by performing a single planning iteration so that the operator only needs to modify the predictions. This could leverage planning approaches such as [31] which use terrain traversability to switch between locomotion modes such as walking with or without hand supports. Another method to reduce operator burden could be to initialize a new key frame to the operator’s posture using a retargeting framework [15, 32]. However while this applies well to standard postures it may be difficult for abnormal postures such as Fig 5(c,d).

Future work will also focus on controllers more capable of executing the motions generated by this framework. For this work we relied on a simple impedance controller for trajectory validation. Recent advancements have been made in applying model-predictive control (MPC) for multi-contact motions on legged robots [33, 34]. We plan to investigate a method for extracting contact sequences and posture profiles from our trajectories which can be consumed by an MPC or similar controller.

A. Acknowledgements

Thanks to Mark Paterson, Alex Sowell and the rest of the NASA JSC team for supporting this effort and in particular enabling joint impedance commands. Thanks to Joseph Godwin for his internship and fabricating test structures.

REFERENCES

- [1] Steve Tonneau et al. “An efficient acyclic contact planner for multipled robots”. In: *IEEE Transactions on Robotics* 34.3 (2018), pp. 586–601.
- [2] Karim Bouyarmane et al. “Multi-contact motion planning and control”. In: *Humanoid Robotics: A Reference* (2018), pp. 1–42.
- [3] Matt Zucker et al. “A general-purpose system for teleoperation of the DRC-HUBO humanoid robot”. In: *Journal of Field Robotics* 32.3 (2015), pp. 336–351.
- [4] Matthew Johnson et al. “Team IHMC’s lessons learned from the DARPA Robotics Challenge: Finding data in the rubble”. In: *Journal of Field Robotics* 34.2 (2017), pp. 241–261.
- [5] Pat Marion et al. “Director: A user interface designed for robot operation with shared autonomy”. In: *The DARPA Robotics Challenge Finals: Humanoid Robots To The Rescue* (2018), pp. 237–270.
- [6] Kourosh Darvish et al. “Teleoperation of Humanoid Robots: A Survey”. In: *arXiv preprint arXiv:2301.04317* (2023).
- [7] Jordan Allspaw, Gregory LeMasurier, and Holly Yanco. “Implementing Virtual Reality for Teleoperation of a Humanoid Robot”. In: *arXiv preprint arXiv:2104.11826* (2021).
- [8] Murphy Wonsick and Taşkın Padır. “Human-humanoid robot interaction through virtual reality interfaces”. In: *2021 IEEE Aerospace Conference (50100)*. IEEE, 2021, pp. 1–7.
- [9] Mohamed Elobaid et al. “Telexistence and teleoperation for walking humanoid robots”. In: *Intelligent Systems and Applications: Proceedings of the 2019 Intelligent Systems Conference (IntelliSys) Volume 2*. Springer, 2020, pp. 1106–1121.
- [10] Steven Jens Jorgensen et al. *cockpit interface for locomotion and manipulation control of the NASA valkyrie humanoid in virtual reality (VR)*. Tech. rep. 2022.
- [11] Adam Eric Leeper et al. “Strategies for human-in-the-loop robotic grasping”. In: *Proceedings of the seventh annual ACM/IEEE international conference on Human-Robot Interaction*. 2012, pp. 1–8.
- [12] Nancy S Pollard et al. “Adapting human motion for the control of a humanoid robot”. In: *Proceedings 2002 IEEE international conference on robotics and automation (Cat. No. 02CH37292)*. Vol. 2. IEEE, 2002, pp. 1390–1397.
- [13] Behzad Dariush et al. “Online transfer of human motion to humanoids”. In: *International Journal of Humanoid Robotics* 6.02 (2009), pp. 265–289.
- [14] Katsu Yamane and Jessica Hodgins. “Control-aware mapping of human motion data with stepping for humanoid robots”. In: *2010 IEEE/RSJ International Conference on Intelligent Robots and Systems*. IEEE, 2010, pp. 726–733.
- [15] Luigi Penco et al. “A multimode teleoperation framework for humanoid loco-manipulation: An application for the icub robot”. In: *IEEE Robotics & Automation Magazine* 26.4 (2019), pp. 73–82.
- [16] Kazuya Otani and Karim Bouyarmane. “Adaptive whole-body manipulation in human-to-humanoid multi-contact motion retargeting”. In: *2017 IEEE-RAS 17th International Conference on Humanoid Robotics (Humanoids)*. IEEE, 2017, pp. 446–453.
- [17] “jMonkeyEngine”. [Online]. Available: <https://jmonkeyengine.org/>. Accessed: 2023-02-15.
- [18] “JavaFX”. [Online]. Available: <https://openjfx.io/>. Accessed: 2023-02-15.
- [19] “Valve Index”. [Online]. Available: <https://www.valvesoftware.com/en/index/>. Accessed: 2023-02-15.
- [20] “HTC Vive”. [Online]. Available: <https://www.vive.com/>. Accessed: 2023-02-15.
- [21] Steven Macenski et al. “Robot Operating System 2: Design, architecture, and uses in the wild”. In: *Science Robotics* 7.66 (2022), eabm6074. DOI: 10.1126/scirobotics.abm6074. URL: <https://www.science.org/doi/abs/10.1126/scirobotics.abm6074>.
- [22] Maurice Fallon et al. “An architecture for online affordance-based perception and whole-body planning”. In: *Journal of Field Robotics* 32.2 (2015), pp. 229–254.
- [23] Patrick Beeson and Barrett Ames. “TRAC-IK: An open-source library for improved solving of generic inverse kinematics”. In: *2015 IEEE-RAS 15th International Conference on Humanoid Robots (Humanoids)*. IEEE, 2015, pp. 928–935.
- [24] David E Orin and Ambarish Goswami. “Centroidal momentum matrix of a humanoid robot: Structure and properties”. In: *2008 IEEE/RSJ International Conference on Intelligent Robots and Systems*. IEEE, 2008, pp. 653–659.
- [25] Francesco Bullo and Richard M Murray. “Proportional derivative (PD) control on the Euclidean group”. In: (1995).
- [26] Twan Koolen et al. “Design of a momentum-based control framework and application to the humanoid robot atlas”. In: *International Journal of Humanoid Robotics* 13.01 (2016), p. 1650007.
- [27] Gino Van Den Bergen. *Collision detection in interactive 3D environments*. CRC Press, 2003.
- [28] Timothy Bretl and Sanjay Lall. “Testing static equilibrium for legged robots”. In: *IEEE Transactions on Robotics* 24.4 (2008), pp. 794–807.
- [29] Romeo Orsolino et al. “Feasible region: An actuation-aware extension of the support region”. In: *IEEE Transactions on Robotics* 36.4 (2020), pp. 1239–1255.
- [30] Pasquale Chiacchio, Yann Bouffard-Vercelli, and François Pierrot. “Force polytope and force ellipsoid for redundant manipulators”. In: *Journal of Robotic Systems* 14.8 (1997), pp. 613–620.
- [31] Yu-Chi Lin and Dmitry Berenson. “Humanoid navigation planning in large unstructured environments using traversability-based segmentation”. In: *2018 IEEE/RSJ International Conference on Intelligent Robots and Systems (IROS)*. IEEE, 2018, pp. 7375–7382.
- [32] Alessandro Di Fava et al. “Multi-contact motion retargeting from human to humanoid robot”. In: *2016 IEEE-RAS 16th international conference on humanoid robots (humanoids)*. IEEE, 2016, pp. 1081–1086.
- [33] Carlos Mastalli et al. “Crocodyl: An efficient and versatile framework for multi-contact optimal control”. In: *2020 IEEE International Conference on Robotics and Automation (ICRA)*. IEEE, 2020, pp. 2536–2542.
- [34] Donghyun Kim et al. “Highly dynamic quadruped locomotion via whole-body impulse control and model predictive control”. In: *arXiv preprint arXiv:1909.06586* (2019).